experiment 20 mL of a 10^{-3} M substrate solution was deoxygenated and cooled at −15 °C. Controlled potential electrolysis was performed within a few hours, with an average current of about 5 mA. Products were analyzed both by cyclic voltammetry and UV–visible spectroscopy.

Electrochemical Oxidation of the Iron σ-Complex 7. The macroelectrolysis was run at −40 °C and 0V. Analysis of the UV–visible spectrum of the solution at room temperature allowed us to estimate a 20% yield in iron(II)–*N*-alkylporphyrin (λ_{max} 418, 446, 460 sh, and 570, 615, 660 nm). The solution was evaporated to dryness, and then the supporting electrolyte was eliminated by flash chromatography (Florisil, Sigma, elution CH_2Cl_2, 1% HCl). After neutralizing the cationic *N*-alkylporphyrin CH_2Cl_2 solution by washing with water and Zn(II) insertion into the free base, the zinc complex **6** was analyzed by UV–visible spectroscopy (λ_{max} 444, 450 sh, 565, 615, 660 nm), mass spectrometry, and ^1H NMR spectroscopy (Table I): mass spectrum 956 (30) (M + 1), 815 (100) Zn(TpClPP).

Conformations of $(\eta^5\text{-}C_5H_5)_2Nb(S\text{-}p\text{-}C_6H_4X)_2^n$ (n = 0, 1): Responsiveness to Para Substituents on Aryl Groups and to d-Electron Count

Marcetta Y. Darensbourg,* Christopher J. Bischoff, Stephen A. Houliston, Magdalena Pala, and Joseph Reibenspies

Contribution from the Department of Chemistry, Texas A&M University, College Station, Texas 77843. *Received February 14, 1990*

Abstract: The balance of factors that determine the S–M–S angle and M–S–R conformational preference have been examined in a systematic study of aryl thiolate derivatives of the bent metallocenes $(\eta^5\text{-}C_5H_5)_2Nb(S\text{-}p\text{-}C_6H_4X)_2^n$, where for n = 0, X = OMe (**2**), Me (**3**), H (**1**), and Cl (**4**), and for n = +1, X = H ($\mathbf{1}^+$) and Cl ($\mathbf{4}^+$). Cyclic voltammographs showed two reversible waves for the Nb(III) → Nb(IV) and Nb(IV) → Nb(V) redox processes whose positions varied uniformly with the Hammett σ parameter of the X substituent. X-ray crystal structure determinations are presented for **2**, **3**, **4**, and $[\mathbf{4}^+][PF_6^-]$ and compared with **1** and $\mathbf{1}^+$ (*Organometallics*, **1989**, *8*, 1315). The S-aryls of Nb(V) complexes (the d^0 derivatives, $\mathbf{1}^+$ and $\mathbf{4}^+$) as well as the d^1 complex **4**, $(\eta^5\text{-}C_5H_5)_2Nb(S\text{-}p\text{-}C_6H_4Cl)_2$, adopt an endo arrangement relative to the cyclopentadienyl rings and have wide S–Nb–S angles of 101.4°, 102.3°, and 98.7°, respectively. Complexes **1**, **2**, and **3** have an exo configuration with aryl groups bent back into the cleft between the Cp rings. The exo isomers have small S–Nb–S angles of 75.4°, 79.1°, and 77.1°, respectively. Complex **2** crystallized in the monoclinic space group $C2/c$, with a = 22.869 (9) Å, b = 6.962 (3) Å, c = 13.951 (4) Å, β = 98.38 (3)°, V = 2197.6 Å^3, and Z = 4. Complex **3** crystallized in the orthorhombic space group $Aba2$, with a = 13.536 (4) Å, b = 22.659 (2) Å, c = 7.017 (3) Å, V = 2152 Å^3, and Z = 4. Complex **4** crystallized in the monoclinic space group $C2/c$, with a = 20.252 (6) Å, b = 9.847 (2) Å, c = 12.403 (4) Å, β = 124.00 (2)°, V = 2050.5 Å^3, and Z = 4. Complex **4**+ crystallized in the triclinic space group $P\bar{1}$, with a = 10.488 (6) Å, b = 10.672 (6) Å, c = 11.226 (8) Å, α = 96.29 (5)°, β = 94.28 (5)°, γ = 112.57 (4)°, V = 1143.8 Å^3, and Z = 2. Details of the structures will be presented and placed in context with other bent metallocene analogues.

Introduction

Recently the molecular structures of the bent metallocenes d^1 $(\eta^5\text{-}C_5H_5)_2Nb(SC_6H_5)_2$ (**1**) and d^0 $(\eta^5\text{-}C_5H_5)_2Nb(SC_6H_5)_2^+$ ($\mathbf{1}^+$)[1] and, later, $(\eta^5\text{-}C_5H_5)_2NbCl_2^+$,[2] for comparison with $(\eta^5\text{-}C_5H_5)_2NbCl_2$,[3] were reported as the first examples of the structural changes resulting from different d-electron counts for identical metal centers. For the latter, oxidation resulted in a large increase in the Cl–Nb–Cl angle of the pseudotetrahedral complex of 12.5° (from 85.6° for the neutral d^1 complex to 98.1° for the d^0 cation). Even more dramatic, as demonstrated below, were the differences observed for the thiolate derivatives. Not only did the S–Nb–S angle change by a remarkable 25°, the largest (by over 12°) known value for a $d^1 \rightarrow d^0$ interchange, but, additionally, there was a $M(SPh)_2$ conformational change from the so-called "exo" to the "endo" form.

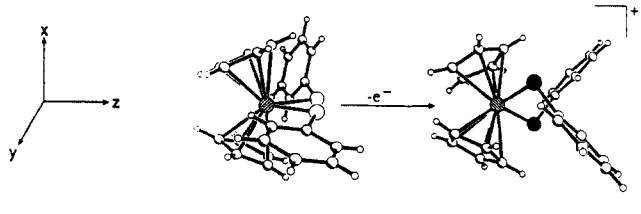

1, "EXO" ∠(S-Nb-S) = 74.9°

$\mathbf{1}^+$, "ENDO" ∠(S-Nb-S) = 101.4°

The configuration change just described was unprecedented in that the analogous light metal neutral derivatives, d^1, $Cp_2V(SPh)_2$ and d^0, $Cp_2Ti(SPh)_2$ whose ∠(S–M–S) are 94.1° and 99.1°, respectively,[4] are isomorphous with the SPh groups of both adopting the "endo" conformation. The titanocene and vanadocene SMe analogues were also structurally characterized with largely the same results.[5] The change in ∠(S–M–S) angle (from 88.7° for d^1, $Cp_2V(SMe)_2$, to 93.7° for d^0, $Cp_2Ti(SMe)_2$) was in the order predicted by established theory,[6,7] and, once again, the endo $M(SR)_2$ conformation was obtained for both of the light metal complexes. In fact, prior to the report of the niobium structures, the only report of an exo orientation of SR groups was that of d^2, $Cp_2Mo(S\text{-}t\text{-}Bu)_2$, whose extremely small ∠(S–Mo–S) of 71° is explained both by electronic (metal based $1a_1$/sulfur lone pair orbital repulsions) and steric (t-Bu/Cp ring repulsions) effects.[8]

Although the configurational change described above (**1**, "EXO" → $\mathbf{1}^+$, "ENDO") is the first example of such with d electron count for the same metal, the possible influence of π-donor ligands on configuration in Cp_2ML_2 complexes was broached by Hoffmann

(1) Darensbourg, M. Y.; Silva, R.; Reibenspies, J.; Prout, C. K. *Organometallics* **1989**, *8*, 1315.
(2) Gowik, P.; Klapotke, T.; Pickardt, J. *Organometallics* **1989**, *8*, 2953.
(3) Prout, C. K.; Cameron, T. S.; Forder, R. A.; Critchley, S. R.; Denton, B.; Rees, G. V. *Acta Crystallogr.* **1974**, *B30*, 2290.
(4) Muller, E. G.; Watkins, S. F.; Dahl, L. F. *J. Organomet. Chem.* **1976**, *111*, 73.
(5) (a) Wark, T. A.; Stephan, D. W. *Organometallics* **1989**, *8*, 2836. (b) Carrondo, M. A. A. F. de C. T.; Jeffrey, G. A. *Acta Crystallogr.* **1983**, *C39*, 42.
(6) Lauher, J. W.; Hoffmann, R. *J. Am. Chem. Soc.* **1976**, *98*, 1729 and references therein.
(7) (a) Alcock, N. W. *J. Chem. Soc. A* **1967**, 2001. (b) Green, J. C.; Green, M. L. H.; Prout, C. K. *J. Chem. Soc., Chem. Commun.* **1972**, 421. (c) Petersen, J. L.; Dahl, L. F. *J. Am. Chem. Soc.* **1974**, *96*, 2248.
(8) Carrondo, M. A. A. F. de C. T.; Matias, P. M.; Jeffrey, G. A. *Acta Crystallogr.* **1984**, *C40*, 932.

0002-7863/90/1512-6905$02.50/0

and Lauher in their 1976 treatise on bent metallocenes, largely in advance of experimental evidence.[6] That work outlined the major role of the bent metallocene frontier $1a_1$ molecular orbital, i.e., that one oriented along the y axis of the Cartesian coordinate system drawn above, and "single-faced" ligand π acceptor or donor orbitals with respect to conformational preferences. More recently Calhorda, Carrondo, and co-workers examined, specifically for thiolate complexes, the factors that determine the configuration with respect to the d^0 and d^2 model complexes $Cp_2M(SH)_2$, M = Ti and Mo.[9] The endo configuration is stabilized by a HS → M π donation (from a sulfur p-type orbital orthogonal to the MSH plane) and thus is clearly favored for complexes in which the metal $1a_1$ orbital is empty, i.e., d^0 complexes. For d^2 complexes the exo configuration avoids the four-electron-destabilizing interaction of filled S orbital–metal $1a_1$ orbital that would exist in the endo form. Extended Hückel calculations showed the endo configuration of $Cp_2Ti(SH)_2$ to be more stable by 0.57 eV over the exo configuration while the d^2 $Cp_2Mo(SH)_2$ complex favored the exo configuration by 0.17 eV over the endo configuration. These calculations were performed maintaining a constant S–M–S angle (95° for Ti and 85° for Mo) which, as we will show below, is an uncomfortable assumption due to the fact that S–M–S angle changes are inextricable from configurational changes. In that work, steric interactions of the form SR/SR, Cp/Cp, and Cp/SR were also considered. Less Cp/SR steric repulsions are experienced in the endo configuration; however, for very bulky R groups, the SR/SR repulsion should drive the structure toward the exo configuration.

The balance of factors that determines S–M–S angle, M–S distances, and conformational preference in $Cp_2M(SR)_2$ complexes is clearly delicate,[9] especially for d^1 complexes which have only recently been addressed in theoretical calculations.[10] Hence we undertook a systematic study of aryl thiolate derivatives of $Cp_2Nb(S\text{-}p\text{-}C_6H_4X)_2$, with aryls substituted in the sterically non-interfering para position by X = OMe, Me, H, and Cl. The electron-releasing/withdrawing capabilities of these groups are known to affect electronic parameters such as HOMO ionization energy and ν(CO) IR position of transition-metal complexes in a systematic way.[11] This series is interesting in that it identifies a large S–M–S angle regime (90–100°) associated with one conformation, endo, and a small angle regime (70–80°) that is accompanied by an exo arrangement of SR groups. Both the largest and the smallest ∠(L–M–L) in d^1 Cp_2ML_2 ever recorded are generated by varying the para substituent on S–Ar, thus suggesting that, in fact, for this series subtle characteristics of the donor ligand and intermolecular packing forces are as controlling of overall geometry as is the metal's d-electron count.

Experimental Section

Methods and Materials. An argon-filled drybox and Schlenk line techniques were used for all compound manipulations and sample transfers. Toluene, tetrahydrofuran (THF), hexane, and pentane were distilled from sodium benzophenone ketyl under nitrogen. Methylene chloride was distilled from P_2O_5 and ethanol was distilled from MgI_2 under nitrogen. Acetone was dried via separation of an acetone/NaI complex from wet acetone, distillation from CaH_2, and storage over molecular sieves. Spectrophotometric grade heptane and triethylamine were degassed with N_2 and stored over molecular sieves. Niobocene dichloride and the para-substituted thiols were obtained from Aldrich Chemical Co. and used without further purification. $[Cp_2Fe][BF_4]$ and $[Cp_2Fe][PF_6]$ were prepared by oxidizing ferrocene with Ph_3CBF_4 or Ph_3CPF_6 in CH_2Cl_2 and washing the dark blue product with ethyl ether.

NMR spectra were obtained on Varian XL 200, XL 200E, and XL 400 spectrometers. Fast atom bombardment mass spectra were recorded on a VG Analytical 70-S mass spectrometer with neutral argon as the bombarding gas at 6–8 keV energy and *m*-nitrobenzyl alcohol as the matrix. Electronic spectra of CH_2Cl_2 and THF solutions were recorded on an IBM 9420 UV–vis spectrometer. The cyclic voltammetry studies were carried out on a Bioanalytical Systems 100A electrochemical analyzer. Potentials were recorded with a Ag°/AgCl reference electrode, a Pt° metal working electrode, and a Pt° wire as the auxiliary electrode. Solutions (THF solvent) were 1 mM in solute and 0.1 M in $[Bu_4N][PF_6]$ electrolyte. Elemental analyses were performed by Oneida Research Services, Inc., Whitesboro, NY, and Galbraith Laboratories, Knoxville, TN.

Syntheses. The synthesis of the $Cp_2Nb(S\text{-}p\text{-}C_6H_4X)_2$ series was carried out as first reported by Giddings[12] for $Cp_2Ti(SC_6H_5)_2$; that of one derivative, $S\text{-}p\text{-}C_6H_4CH_3$, and its subsequent oxidation, is given below in detail. Others were prepared analogously with similar yields. Elemental analyses were acceptable for all and along with mass spectral data may be found in the Supplementary Material.

$[Cp_2Nb(S\text{-}p\text{-}C_6H_4CH_3)_2]$ (3). Into a 100-mL Schlenk flask was placed 0.294 g (1.00 mmol) of Cp_2NbCl_2, 0.280 g (2.00 mmol) of $HS\text{-}p\text{-}C_6H_4CH_3$, 10 mL of triethylamine, and 30 mL of toluene. The solution was stirred for 30 min and refluxed for 1 h. A color change from brown to deep violet occurred after stirring ca. 10 min. The solution was filtered through alumina and the solvent removed under reduced pressure. Addition of 15 mL of toluene and 50 mL of pentane produced a dark green microcrystalline solid that was then recrystallized from toluene/heptane to yield 0.285 g (56% yield) of product. Comparable yields were obtained from the reaction of Cp_2NbCl_2 with the sodium thiolate salts in ethanol or THF. After removal of solvent, the compound was extracted into toluene, filtered through Celite, and crystallized as above. The NaSAr salts were obtained by reaction of the thiol and sodium metal in THF.

$[Cp_2Nb(S\text{-}p\text{-}C_6H_4CH_3)_2][BF_4]$ (3^+). A 100-mL Schlenk flask was loaded with 0.200 g (0.43 mmol) of **3** and 0.120 g (0.44 mmol) of $[Cp_2Fe][BF_4]$. After addition of 20 mL of methylene chloride, an immediate color change from violet to maroon occurred. The solution was stirred for 30 min and 50 mL of pentane added. The resulting maroon crystals were collected on a filter frit, washed twice with 5-mL aliquots of pentane, and dried in vacuo.

Acceptable elemental analyses for $Cp_2Nb(S\text{-}p\text{-}C_6H_4X)_2$ where X = NH_2 and NO_2 have not been obtained. The cyclic voltammetry data for these complexes, presented in Table II, were measured on samples taken from the reaction mixture after the filtration procedure.

X-ray Crystal Structure Determination. Collection and Reduction of X-ray Data. Crystals for structural analysis were grown from toluene solutions layered with heptane in the cases of **2**, **3**, and **4** and from a dilute acetone solution layered with heptane for 4^+. The solutions were allowed to stand at room temperature for 3–4 days for **2**, **3**, and **4** while 4^+ required 6–7 days in order to obtain suitable crystals. Crystals for **2**, **4**, and 4^+ were mounted in capillary tubes and sealed while **3** was mounted on a glass fiber with vacuum grease and cooled to 193 K in a nitrogen cold stream. Details of the crystallographic data collection and refinement for compounds **2**, **3**, **4**, and 4^+ are summarized in Table I. For all compounds, preliminary examination and data collection were performed on a Nicolet R3m/V X-ray diffractometer[15] with Mo Kα (λ = 0.71073 Å) radiation and an oriented graphite crystal monochromator. The diameter of the collimated X-ray beam was 1.0 mm. The 2θ range was 4.0° to 50.0°. Background measurements were performed by stationary crystal and stationary counter techniques at the beginning and end of each scan for one-half of the total scan time. Three standards were collected every 97 reflections. Lorentz and polarization corrections were applied to the data. A 10% decay in the intensity of the control reflections was observed in the case of **4** and 15% decay for 4^+. The intensities of the data set were corrected by employing a correction curve based on the intensity decay of the control reflections. For **2** and **3** no absorption correction was applied; for **4** a face indexed numerical[16] ab-

(9) Calhorda, M. J.; Carrondo, M. A. A. F. de C. T.; Dias, A. R.; Frazao, C. F.; Hursthouse, M. B.; Simoes, J. A. M.; Teixeira, C. *Inorg. Chem.* **1988**, *27*, 2513.
(10) Hall, M. B.; Simpson, C. Q. Manuscript in preparation.
(11) Ashby, M. T.; Enemark, J. H.; Lichtenberger, D. L. *Inorg. Chem.* **1988**, *27*, 191.
(12) Giddings, S. A. *Inorg. Chem.* **1967**, *6*, 849.
(13) *International Tables for X-Ray Crystallography*; Hahn, T., Ed.; D. Reidel Publishing Co: Dordrecht, Holland; Distributed by Kluwer Academic Publishers, 1987; Vol A, pp 101–709.
(14) Residuals: $R_{int} = [\sum F^2 - (F_{mean})^2]/[\sum F^2]$; $R = \sum|F_o - F_c|/\sum F_o$; $wR = [[\sum w(F_o - F_c)^2]/[\sum w(F_o)^2]]^{1/2}$; $S = [[\sum w(F_o - F_c)^2]/[N_{data} - N_{parameters}]]^{1/2}$.
(15) Diffractometer control software, P3VAX 3.42, supplied by Nicolet Analytical X-ray Instruments, Madison WI, U.S.A.

Table I. Crystallographic Data

	2	3	4	4^+
mol formula	$C_{24}H_{24}O_2S_2Nb$	$C_{24}H_{24}S_2Nb$	$C_{22}H_{18}S_2Cl_2Nb$	$C_{22}H_{18}S_2Cl_2NbPF_6$
formula wt, g/mol	501.5	469.5	510.3	655.3
crystal color, habitat	dark green block	dark red needle	dark purple plate	dark purple plate
crystal dimens, mm	0.24 × 0.28 × 0.36	0.10 × 0.18 × 0.44	0.12 × 0.32 × 0.36	0.12 × 0.32 × 0.36
setting angles, deg	$2\theta_{av}$ = 16.1	$2\theta_{av}$ = 21.7	$2\theta_{av}$ = 29.4	$2\theta_{av}$ = 19.67
crystal system	monoclinic	orthorhombic	monoclinic	triclinic
space group[13]	*C*2/*c*	*Aba*2	*C*2/*c*	*P*1
a, Å	22.869 (9)	13.536 (4)	20.252 (6)	10.488 (6)
b, Å	6.962 (3)	22.659 (2)	9.847 (2)	10.672 (6)
c, Å	13.951 (4)	7.017 (3)	12.403 (4)	11.226 (8)
α, deg				96.29 (5)
β, deg	98.38 (3)		124.00 (2)	94.28 (5)
γ, deg				112.57 (4)
V, Å^3	2197.6 (14)	2152 (2)	2050.5 (9)	1143.8 (12)
Z	4	4	4	2
ρ(calcd), g cm^{-3}	1.516	1.449	1.653	1.903
radiation		Mo Kα (λ = 0.71073 Å)		
temp, K	296	193	296	296
scan type	ω (Wyckoff)	θ–2θ	θ–2θ	θ–2θ
variable scan rate, deg/min	2.00–15.00	1.50–15.00	1.50–15.00	1.50–15.00
no. of reflcns collected	2214	1852	2017	4242
obsd reflcns	1770	820	1515	3398
	$\|F\| \geq 2.5\sigma\|F\|$	$\|F\| \geq 2.0\sigma\|F\|$	$\|F\| \geq 2.5\sigma\|F\|$	$\|F\| \geq 4.0\sigma\|F\|$
unique reflcns[14]	1948 (R_{int} = 2.07%)	862	1810 (R_{int} = 3.45%)	4018 (R_{int} = 1.70%)
absorption coeff, mm^{-1}	0.723	0.727	1.026	1.043
index ranges	$-27 \leq h \leq 26$; $0 \leq k \leq 8$; $0 \leq l \leq 16$	$0 \leq h \leq 16$; $-17 \leq k \leq 0$; $0 \leq l \leq 8$	$-20 \leq h \leq 24$; $0 \leq k \leq 11$; $-14 \leq l \leq 0$	$-12 \leq h \leq 12$; $-12 \leq k \leq 12$; $-13 \leq l \leq 0$
data to parameter ratio	13.4:1	6.6:1	12.2:1	10.5:1
R,[14] %	3.12	2.96	7.75	6.59
wR,[14] %	4.36	4.36	7.70	9.20
S[14]	1.09	1.20	3.47	2.26
largest, mean Δ/σ final	0.002, 0.001	0.001, 0.001	0.017, 0.001	1.81, –0.033
largest pos. neg. peak, e$^-$/Å^3	0.27, –0.25	0.58, –0.41	1.32, –1.18	2.25, –1.07
g ($w^{-1} = (\sigma F)^2 + gF^2$)	0.0010	0.0010	0.0001	0.0010

sorption correction was applied where T_{max} = 0.9880 and T_{min} = 0.9679; and for 4^+ a semiempirical[17] absorption correction was applied where T_{max} = 0.8941 and T_{min} = 0.7175. Data were smoothed by a learnt peak profiling technique.[18]

Solution and Refinement. The molecular structures were solved by direct methods[19] and refined with a full-matrix least-squares method [quantity minimized $\sum w(F_o - F_c)^2$, where $w^{-1} = (\sigma F)^2 + gF^2$]. All non-hydrogen atoms were refined anisotropically for **2**, **3**, and **4**. For 4^+ all non-hydrogen atoms for the cation were refined anisotropically. Hydrogen atoms for all structures were placed in idealized positions and their individual isotropic thermal motion was fixed at 0.08. Neutral atom scattering factors and anomalous scattering correction terms were taken from a standard source.[20,21] For **3**, the Rodgers absolute configuration parameter η was refined to 1.1 (6) indicating the correct configuration.[22] In **3** and **4**, the extinction coefficient χ[23] was refined to 0.00023 (13) and 0.00030 (11), respectively, where $F = F_c/[1 + 0.002\chi F_c^2/\sin(2\theta)]^{0.25}$.

The anion of 4^+ was found to be disordered between two positions. The disordered anion can be generated by fixing a rotation axis through F1a, P, and F4a and rotating the original anion by 46° around the axis. The site occupation factors for the two configurations were refined together. A ratio of site occupation of 78% (F2a, F3a, F5a, F6a) to 22% (F2b, F3b, F5b, F6b) was calculated. The site occupation factor for F1a, P, and F4a was fixed at 100%. The three largest peaks in the final Fourier difference map (2.25 e$^-$ Å^{-3} 0.56 Å from P, 1.46 e$^-$ Å^{-3} 1.19 Å from F5a, and 0.90 e$^-$ Å^{-3} 0.82 Å from F3b), the largest Δ/σ shift (1.81 for z/c F3a), and the high weighted residual value are most probably due to discrepancies in modeling the disorder of the anion. Attempts at modeling more than two disordered anions failed. Finally the intramolecular distances were constrained to idealized values and the structure of 4^+ was refined to convergence.

Results and Discussion

Synthesis and Characterization. Neutral $Cp_2Nb(SAr)_2$ complexes were readily prepared by thiolate/halide exchange and oxidation was equally well-effected in all cases of S-*p*-C_6H_4X by the ferrocenium cation. All are darkly colored (purple to green-black) crystalline solids and are thermally stable to 150 °C. The fast atom bombardment mass spectra of $Cp_2Nb(SAr)_2$ showed the parent ion and loss of one SAr group as principal peaks for all compounds (Table XXVS, Supplementary Material). Peaks assignable to Cp_2Nb^+ were observed for all samples at lower intensities, ca. 10%, as were peaks of masses consistent with the interaction of oxygen, presumably from the matrix, with M^+ – L and M^+ – 2L fragments. Unassigned low-intensity peaks (<10%) of mass M^+ – L – 34 and M^+ – (L + 34) – 15 were also found. In no spectra were there indications of Cp group loss or significant fragmentation of the S-bound ring. For X = Cl, the expected isotope effect for natural abundance level of ^{35}Cl and ^{37}Cl was observed for M^+ and M^+ – L. That is, the observed ratio of peaks at M^+ masses 513, 511, and 509 of 1:4.4:5.6 agree with the calculated ratio of 1:4.1:5.4 based on the natural abundance of ^{35}Cl, ^{37}Cl, ^{13}C, ^{33}S, ^{34}S, and ^2H.

The ^1H NMR spectra of $Cp_2Nb(S\text{-}p\text{-}C_6H_4X)_2^+$ were recorded in acetone-d_6 solutions for both the PF_6 and BF_4 salts. No counterion effect was observed. All spectra comprise, apart from signals of the X substituent, a singlet due to the protons of cyclopentadienyl rings in the region 6.62–6.73 ppm and two doublets assigned to phenyl ring protons with chemical shifts in the range of 7.11 to 7.59 ppm. A consistent, though small, shift of the Cp signal to higher field is observed with increased shielding character of the para substituent in the order Cl < H < CH_3 < OCH_3 (Table XXVIS, Supplementary Material). The phenyl region shows a typical AB pattern and, not surprisingly, a much more pronounced substituent effect. For X = OCH_3, the phenyl ring protons appear as two doublets at 7.11 and 7.46 ppm, with a coupling constant of 9.0 Hz. The lower field signal, in this and other spectra, is assigned to protons in the ortho position relative to sulfur. This assignment is substantiated by observed changes in the chemical

(16) Busing, W. R.; Levy, H. A. *Acta Crystallogr.* **1957**, *10*, 180.
(17) North, A. C. T.; Phillips, D.; Mathews, F. S. *Acta Crystallogr.* **1968**, *A24*, 351.
(18) Diamond, R. *Acta Crystallogr.* **1969**, *A25*, 43.
(19) All crystallographic calculations were performed with SHELXTL-PLUS rev 3.4 (G. M. Sheldrick, Institut für Anorganische Chemie der Universität, Tammannstrasse 4, D-3400, Göttingen, Federal Republic of Germany) supplied by Nicolet Analytical X-ray Instruments, Madison WI, U.S.A., on a MicroVaxII minicomputer.
(20) *International Tables for X-Ray Crystallography*; Ibers, J. A., Hamilton, W. C., Eds.; Kynoch Press: Birmingham, England, 1974; Vol IV, p 99.
(21) Reference 20, p 149.
(22) Rodgers, D. *Acta Crystallogr.* **1981**, *A37*, 734.
(23) Larson, A. C. *Acta Crystallogr.* **1967**, *A23*, 604.
(24) Gould, E. S. *Mechanism and Structure in Organic Chemistry*; Holt, Rinehart and Winston: New York, 1959; p 223.

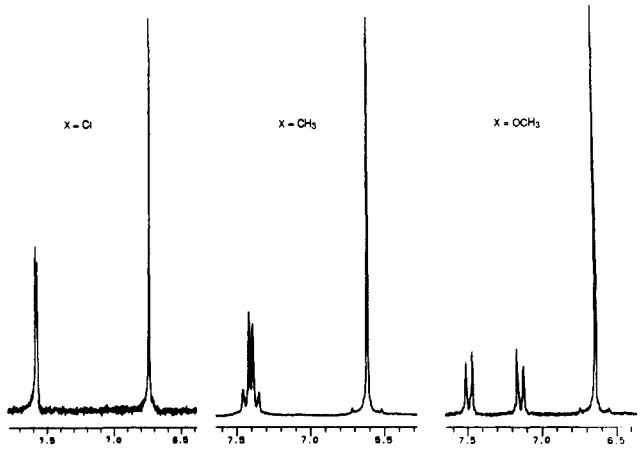

Figure 1. ^1H NMR, in acetone-d_6, of $[Cp_2Nb(S\text{-}p\text{-}C_6H_4X)_2][BF_4]$ where X = Cl, CH_3, and OCH_3.

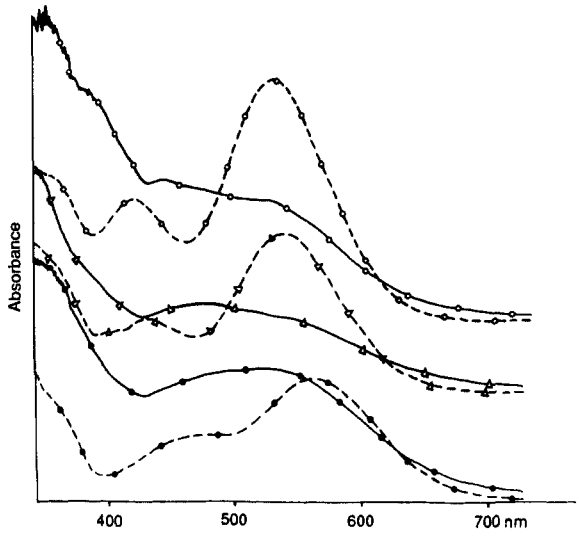

Figure 2. Electronic spectra of $Cp_2Nb(S\text{-}p\text{-}C_6H_4X)_2$ in CH_2Cl_2 for the neutral (solid lines) and cationic (dashed lines) complexes: (○) X = Cl, (△) X = CH_3, (●) X = OCH_3.

shifts with the change of substituents. The more electron withdrawing the X group, the more deshielded, and shifted downfield, is the upperfield signal in the phenyl region, whereas the lower field doublet shifts only slightly (Figure 1). The singlet due to Cp ring protons in $[Cp_2Nb(S\text{-}p\text{-}C_6H_4OCH_3)_2][BF_4]$ was sharp over the temperature range of −85 to +30 °C.

The ^{13}C [^1H] NMR spectrum of $[Cp_2Nb(S\text{-}p\text{-}C_6H_4Cl)_2][BF_4]$ in methylene-d_2 chloride showed resonances at 113.7 ppm (Cp carbons), 130.0 and 133.3 ppm (C_6, C_7, C_9, and C_{10} aryl carbons), and 135.3 and 142.9 ppm (C_8 and C_{11} aryl carbons). More precise assignments are not possible at this time.

The electronic spectra of the d^0 complex cations, $Cp_2Nb(S\text{-}p\text{-}C_6H_4X)_2^+$, show two main features in the visible region, and a shoulder at ca. 350 nm is seen on the intense charge transfer band below 300 nm (Figure 2). The visible region bands are well separated and strong (e.g., for $[Cp_2Nb(S\text{-}p\text{-}C_6H_4OCH_3)_2][BF_4]$ in THF solution ϵ = 4500 and 2100 M^{-1} cm^{-1} for the bands at λ = 550 and 456 nm, respectively). In each case the visible band of highest λ_{max} value is the more intense and there is a systematic bathochromic shift of both higher wavelength bands as the electron-donating ability of the aryl substituent increases. Although the band pattern and resolution is the same, there is a slight (10–15 nm) shift to the blue on changing the solvent from CH_2Cl_2 to THF.

For the neutral analogues, d^1 $Cp_2Nb(S\text{-}p\text{-}C_6H_4X)_2$, the visible region consists of an ill-defined broad envelope, (Figure 2), and hence the λ_{max} values given in Table XXVIS (Supplementary Material) are a rather arbitrary selection of maxima. Like the cationic analogues the absorptions for the neutral complexes are

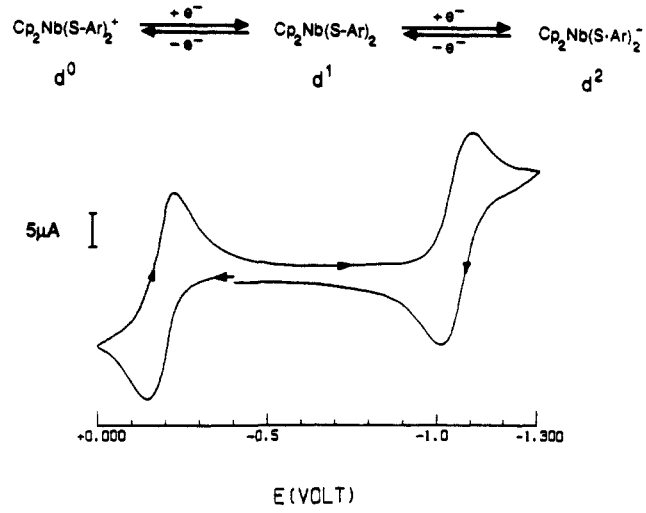

Figure 3. Cyclic voltammograph of 10^{-3} M $Cp_2Nb(S\text{-}p\text{-}C_6H_4CH_3)_2$ in THF with 0.1 M $[n\text{-}Bu_4N][PF_6]$ as supporting electrolyte.

Table II. Comparison of Hammett σ Parameters and Redox Potentials of $Cp_2Nb(S\text{-}p\text{-}C_6H_4X)_2$ from Cyclic Voltammographs

		$E_{p_{av}}$, V	
X	σ^a	Nb(V) → Nb(IV)	Nb(IV) → Nb(III)
NO_2	0.78	0.09	−0.78
Cl	0.23	−0.09	−0.94
H	0.00	−0.14	−1.00
CH_3	−0.17	−0.18	−1.05
OCH_3	−0.27	−0.21	−1.08
NH_2	−0.66	−0.33	−1.21

[a] σ values taken from ref 24.

strong (e.g. for $Cp_2Nb(S\text{-}p\text{-}C_6H_4OCH_3)_2$ in THF, ϵ = 1900 M^{-1} cm^{-1} at 510 nm) and a blue shift is observed with decrease of electron-donating ability of the para substituents. The lower energy component(s) is similar in position (but weaker) to that of the oxidized analogues. The higher energy component is shifted to longer λ from the corresponding band in the cations.

An appropriate comparison of these data is to be found with the Cp_2TiX_2 series whose electronic properties have been extensively probed.[25] Bands of similarly high intensities (ϵ on the order of 1–5 × 10^3) as those seen above are assigned to ligand-to-metal charge-transfer absorptions and the assignments are corroborated by photochemical studies. Once again a red shift was observed as the electron-donating ability of X increased; however, the lowest energy transitions for X = F and Cl are assigned to Cp → Ti charge transfer, for X = I and CH_3, to X → Ti charge transfer, and assignments (Cp → Ti or X → Ti) are ambiguous for X = Br. The implication is that considerable delocalization of the HOMO/LUMO encompasses both the organometallic and the X ligand. The unusually high intensity and broad shapes of the bands in the niobium thiolates also suggest an assignment of ligand → Nb charge-transfer transitions; however, it is not possible to define the ligand, Cp or thiolate, with confidence.

Electrochemistry. All complexes, $Cp_2Nb(SAr)_2$ and $Cp_2Nb(SAr)_2^+$, show two reversible one-electron processes, assigned as indicated on the typical voltammograph in Figure 3. (There is no indication that the redox process takes place on the SAr ligand based on the comparison of voltammographs of the thiols and thiolates which show sharp, intense ring reductions (~ −1 V) and oxidations (~ +1 V)). The anionic d^2 product shown in Figure 3, $Cp_2Nb(SAr)_2^-$, is a presumed formulation. It has not been isolated in preliminary attempts at bulk chemical (Na°/Hg amalgam or Na°/naphthalenide) reduction.[26]

The average values of the reduction and oxidation wave potential maxima, $E_{p_{av}}$, for the series of $Cp_2Nb(S\text{-}p\text{-}C_6H_4X)_2$ are presented

(25) (a) Bruce, M. R. M.; Tyler, D. R. *Organometallics* **1985**, *4*, 528. (b) Bruce, M. R. M.; Kenter, A.; Tyler, D. R. *J. Am. Chem. Soc.* **1984**, *106*, 639.
(26) Darensbourg, M. Y.; Houliston, S. A.; Pala, M. Unpublished results.

Table III. Selected Intramolecular Distances and Bond Angle Data for $Cp_2Nb(S\text{-}p\text{-}C_6H_4X)_2$ and $[Cp_2Nb(S\text{-}p\text{-}C_6H_4X)_2][PF_6]$

	1 X = H[a]	**2** X = OCH_3	**3** X = CH_3	**4** X = Cl	**1**$^+$ X = H^+	**4**$^+$ X = Cl^+
Nb–S, Å	2.516 (7)	2.513 (1)	2.522 (3)	2.509 (3)	2.417 (1)	2.406 (3) 2.420 (3)
S–C_{11}, Å	1.78 (1)	1.774 (3)	1.777 (6)	1.765 (8)	1.783 (5)	1.765 (8) 1.788 (8)
S···S, Å	3.080	3.202	3.143	3.807	3.741	3.758
Cp–Nb_{av}, Å	2.43 (1)	2.41 (2)	2.40 (2)	2.38 (3)	2.41 (2)	2.41 (2)
S–Nb–S, deg	75.4 (9)	79.1 (1)	77.1 (1)	98.7 (1)	101.4 (1)	102.3 (1)
Cp–Nb–Cp,[b] deg	132.4	132.5	131.9	130.1	131.6	131.4
Nb–S–C_{11}, deg	111 (4)	110.6 (1)	109.8 (2)	117.6 (3)	112.0 (1)	114.5 (2) 110.9 (2)

[a] Average of lengths and angles for two independent molecules in unit cell. [b] $Cp_{(centroid)}$–Nb–$Cp_{(centroid)}$ angles.

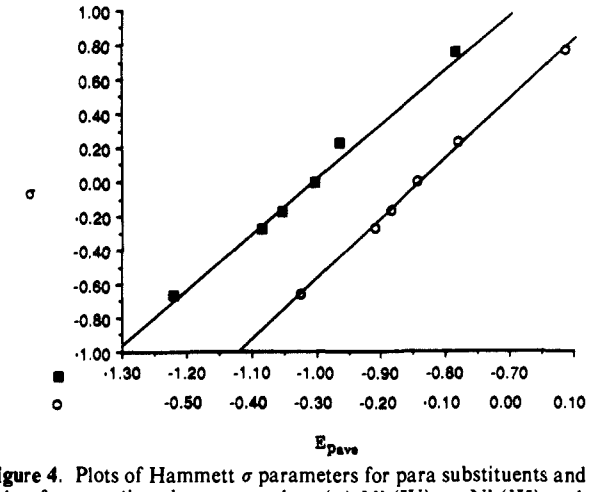

Figure 4. Plots of Hammett σ parameters for para substituents and $E_{p_{av}}$ value from cyclic voltammographs: (■) Nb(IV) → Nb(III) and (○) Nb(V) → Nb(IV).

in Table II. Plots of the Hammett σ values for the para substituents and the $E_{p_{av}}$ of both redox waves resulted in linear correlations of nearly identical slopes (Figure 4). The better electron donating groups thus facilitate oxidation or the ease with which electrons are removed, equally from the Nb(III) or Nb(IV) complexes, while electron withdrawing substituents facilitate the uptake of electrons by Nb(V) or Nb(IV) complexes in a uniform manner. This result is consistent with the dependence of the He I photoelectron spectra of the HOMO ionization found for the $CpFe(CO)_2(S\text{-}p\text{-}C_6H_4X)$ series.[11]

Crystallography. Atomic coordinates of **2**, **3**, **4**, and **4**$^+$ are available as Supplementary Material, and thermal ellipsoid plots are shown in Figures 5–8. Table III lists selected bond distances and angles for $Cp_2Nb(S\text{-}p\text{-}C_6H_4X)_2$ and $Cp_2Nb(S\text{-}p\text{-}C_6H_4Cl)_2^+$ complexes presented in this work as well as those from the earlier study[1] of $Cp_2Nb(SC_6H_5)_2$ and $Cp_2Nb(SC_6H_5)_2^+$. No unusual bond lengths or bond angles in Cp and phenyl rings were observed. A full listing of bond lengths and bond angles for all new structures as well as packing diagrams and complete lists of calculated and observed structure factors and anisotropic displacement coefficients are available as supplementary material.

In all structures, the niobium metal is in a distorted tetrahedral field of cyclopentadienyl (Cp) and sulfur donor ligands. The Cp rings are staggered by 15° to 18° relative to each other and the angle between the Cp centroids and metal is in the 130–132° range for all compounds (Table III). The aryl thiolate ligands assume one of two conformations relative to the Cp_2Nb fragment. In the exo conformation the S–C(11) bonds are directed away from the z axis and into the yz plane whereas in the endo conformation the S–C(11) bonds are arranged more or less parallel to the x axis (see Introduction for axes orientation).

The complexes in the exo conformation, **1**, **2**, and **3**, have S–Nb–S angles <80°. The effects of the electron-releasing substituents on the S–Nb–S angles as compared to H are minor. The Nb–S–C(11) angles for X = OMe, Me, and H are also all similar at ca. 110° whereas a significantly larger angle is observed for X = Cl. All Nb–S bond distances of the d^1 derivatives, including the chloro derivative, are statistically the same.

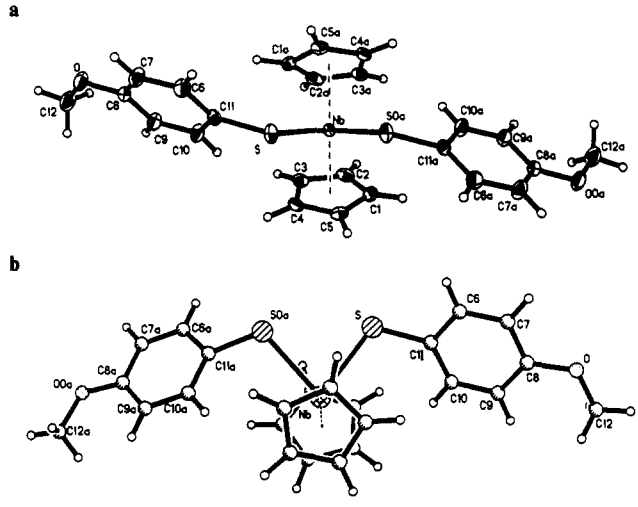

Figure 5. (a) Thermal ellipsoid plot (50% probability) of $Cp_2Nb(S\text{-}p\text{-}C_6H_4OCH_3)_2$. Hydrogen atoms are placed in idealized positions. (b) Alternate view of the molecular structure of **2**.

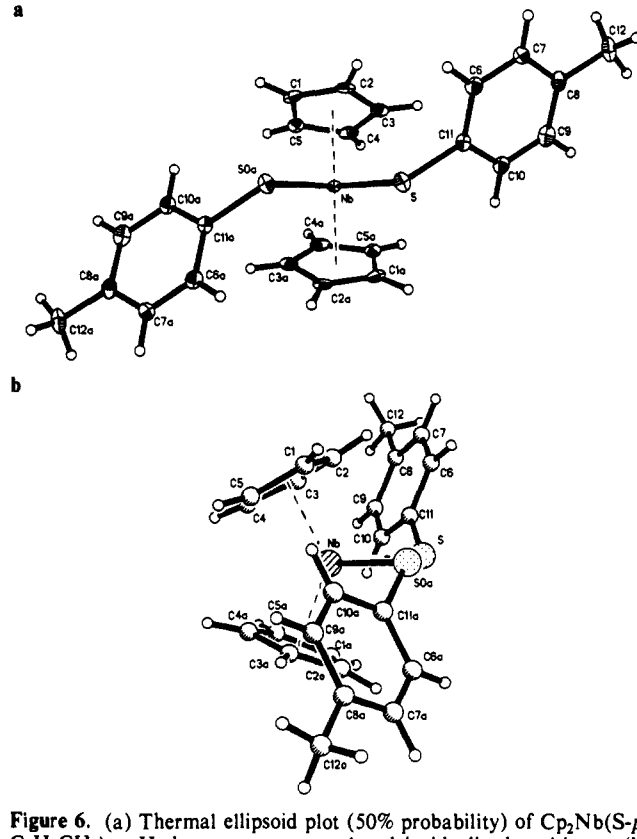

Figure 6. (a) Thermal ellipsoid plot (50% probability) of $Cp_2Nb(S\text{-}p\text{-}C_6H_4CH_3)_2$. Hydrogen atoms are placed in idealized positions. (b) Alternate view of the molecular structure of **3**.

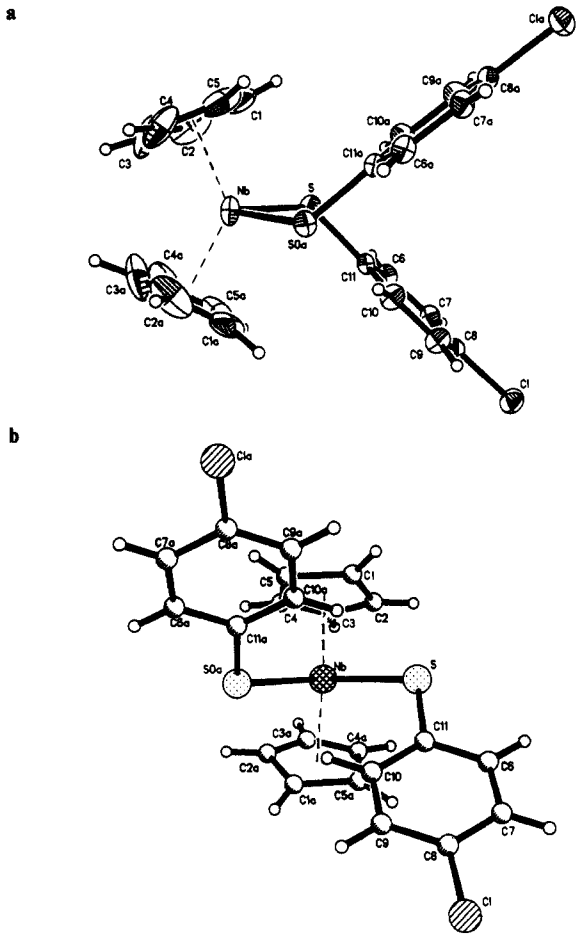

Figure 7. (a) Thermal ellipsoid plot (50% probability) of $Cp_2Nb(S\text{-}p\text{-}C_6H_4Cl)_2$. Hydrogen atoms are placed in idealized positions. (b) Alternate view of the molecular structure of **4**.

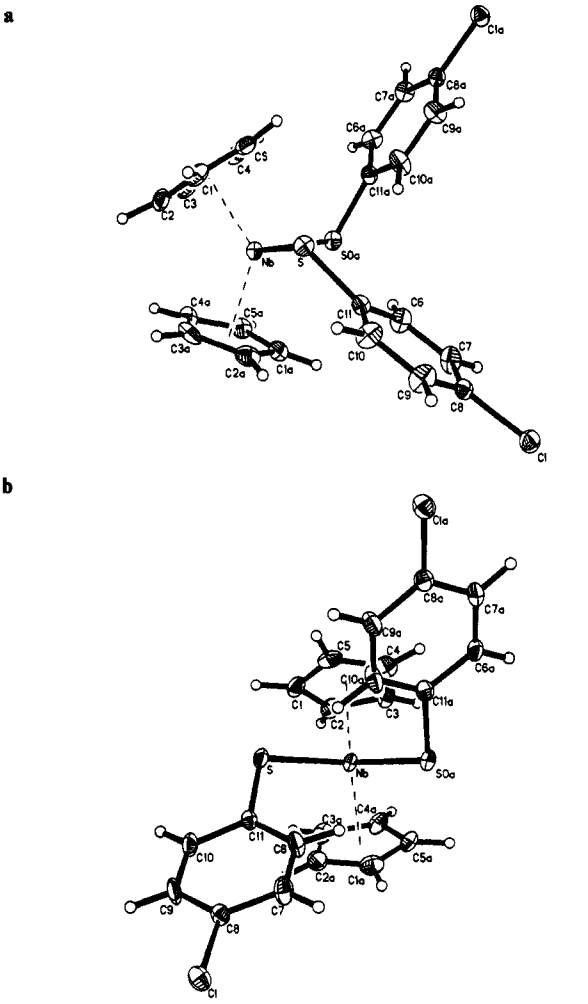

Figure 8. (a) Thermal ellipsoid plot (50% probability) of $[Cp_2Nb(S\text{-}p\text{-}C_6H_4Cl)_2][PF_6]$. Hydrogen atoms are placed in idealized positions. (b) Alternate view of molecular structure of $\mathbf{4}^+$.

The S-aryl groups of both the neutral and oxidized forms of $Cp_2Nb(S\text{-}p\text{-}C_6H_4Cl)_2$ are in the endo conformation. The very large S-Nb-S angle of 98.7 (1)° for the d^1 complex is only 3.6° smaller than that of the cationic d^0 complex, 102.3 (1)°. The Nb-S distances are significantly shorter, roughly 0.1 Å, for the d^0 complexes $\mathbf{1}^+$ and $\mathbf{4}^+$ as compared to their d^1 complex analogues, regardless of conformation.

Severe disorder prevented complete refinement of the PF_6 anion in the $[Cp_2Nb(S\text{-}p\text{-}C_6H_4Cl)_2][PF_6]$ structure; however, the anion appears to be more closely interacting with one aryl group than the other. Assuming a P-F distance of 1.5 Å,[1] the distance between P of the anion and the closer Cl of the cation, 4.06 Å, suggests that the Cl and F are precisely at their van der Waals contact distance.

As a result of the small S-Nb-S angles in the exo configuration, the sulfur-sulfur distances are also short. While well beyond a S-S covalent bond distance (ca. 2.04 Å) the distances presented in Table III for the exo structures, **1**, **2**, and **3**, are within the S···S van der Waals contact distance of ca. 3.60 Å whereas the endo structures **4**, $\mathbf{4}^+$, and $\mathbf{1}^+$ have larger S···S distances.

As will be shown below, the energy differences between conformations in the d^1 Nb(IV) bent metallocenes are small and probably greatly influenced (if not in some cases determined) by crystal packing forces, the result of which might also reasonably account for the minor differences seen between structures with the same general conformation. In view of the fact that the $Cp_2Nb(S\text{-}p\text{-}C_6H_4X)_2$ series was prepared to minimize steric differences while changing electronic factors, we have examined the structural variations for possible correlation to the substituents on the thiolate ligands. These subtle differences within the two classes of structures are best represented in Newman projections (Figure 9). View A (exo) is of the C(11)-S-Nb-S(0a) torsion angle viewed down the S-Nb bond. This projection represents the amount of bending of the phenyl rings out of the S-Nb-S plane. Should the C(11)-S-Nb-S(0a)-C(11a) lie in one plane for the exo conformation the torsion angle would be 180°. In fact, ab initio molecular orbital calculations on a sterically unencumbered model of $Cp_2Nb(SH)H$ show minimum energy at this exo configuration.[10] In such a configuration the electronic factors favor the exo configuration over the endo configuration (maximum energy with a torsion angle of 90°) by approximately 28 kcal/mol.[10] Since the smallest torsion angle is observed for the X = Me derivative, 146.8°, rather than the better electron donating OCH_3 derivative, 163.9° (which is close to the unsubstituted or H derivative (166.8°)), it would appear that electronic factors are not determining the deviations. On the other hand the packing diagrams (Supplementary Material) of **2** and **3** show close contacts between Cp hydrogens and the sulfur atoms of adjacent molecules to the extent of 2.74 and 2.71 Å, respectively. Such dipolar type interactions could determine the observed torsion angles; i.e., the intermolecular contacts are more likely causes than intramolecular differences in bonding.

The C(6)-C(11)-S-Nb torsion angle shows the amount of twist the aryl moiety experiences relative to the C(11)-S-Nb plane (Figure 9, view B (exo)). The aryl ring twisting is due to the steric interactions between the Cp ring protons and the aryl ring which occur as a result of the bending from C(11)-S-Nb-S(0a)-C(11a) planarity described above and hence follows the same order, X = H < OCH_3 < Me.

The analysis of similar differences in the endo conformers (Figure 9, views C and D) follows assuming that the determinant of conformation is the overlap between a filled sulfur lone pair, 3p-type orbital and the Nb $1a_1$ orbital. An optimization of this interaction in the simple d^0 $Cp_2Nb(SH)H^+$ model by ab initio

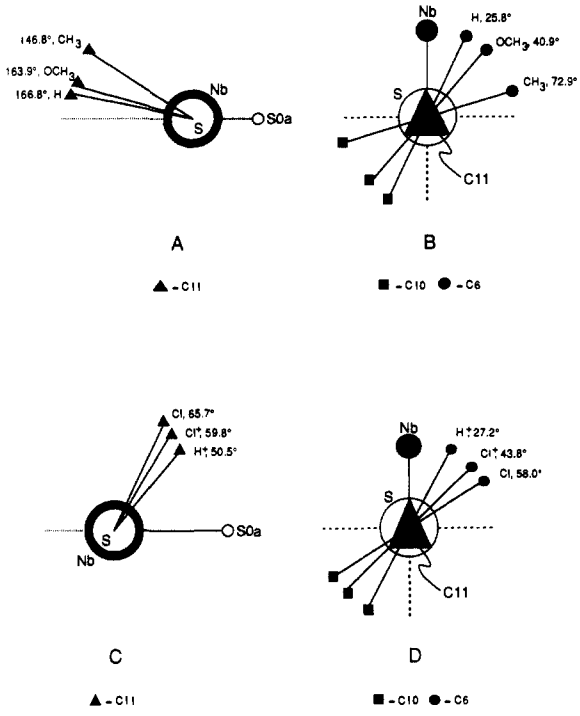

Figure 9. The dihedral angles C11–S–Nb–S0a and C6–C11–S–Nb for the exo conformers, views A and B, respectively, and the endo conformers, views C and D, respectively.

molecular orbital calculations results in a predicted H–S–Nb–H torsion angle of 74°.[10] The differences between the calculated and the experimental values in Figure 9 may be accounted for on the basis of steric effects superimposed on this electronic preference. That is, larger angles result in more Cp hydrogen/aryl ring steric repulsion. The deviation to smaller torsion angles relieves such steric interaction; this is emphasized in the cationic complexes $\mathbf{1}^+$ and $\mathbf{4}^+$ where Nb–S distances are shorter than in the neutral analogue, **4**. Figure 9 view D (endo) is the rotation of the aryl ring, represented by the C(6)–C(11)–C(10) plane rotating about the C(11)–S bond. Once again molecular models suggest the aryl ring twist to be in relief of steric interactions between the Cp ring protons and the aryl ring, hence the smaller angle in view C results in a smaller angle in view D. There are no close contacts between metallocene units (i.e., Cp hydrogens to sulfur sites) as was seen for the exo conformers.

Concluding Comments. The collection of structural data of all known $Cp_2M(SAr)_2$ structures to date found in Table IV is notable in that they are divided into a group of wide-angle endo conformers, thusfar always observed for d^0 configurations and sometimes for d^1, and a second group of small-angle exo conformers, preferred for some d^1 complexes and the one structurally characterized d^2 complex. The endo conformer, having less Cp–SR steric repulsion and maximum S lone pair overlap with the metal-based $1a_1$ orbital, is clearly the preferred conformer for d^0 complexes. The preference of the d^1 complexes $Cp_2V(SR)_2$ for the endo configuration may be ascribed to a combination of factors: minimum steric repulsions and weaker π repulsion (in comparison to the more diffuse Nb cogener). In the case of d^2, $Cp_2Mo(S\text{-}t\text{-}Bu)_2$, both the filled $1a_1$–S lone pair orbital interaction as well as the SR–SR steric interaction are clearly repulsive, generating the exo conformer. Since the aryl rings present relatively small steric interactions with Cp, we conclude that the electronic factor must dominate for the more electron diffuse d^1 niobium analogues.

We are then left to account for the curious nature of the d^1 niobium derivative which adopts the endo configuration, $Cp_2Nb(S\text{-}p\text{-}C_6H_4Cl)_2$. There are no close intermolecular interactions that would account for this. Steric differences in our series are negligible. The uniform effect of the para substituent on various solution parameters of $Cp_2Nb(S\text{-}p\text{-}C_6H_4X)_2$ has been noted and suggests that either all complexes have the same structure in solution, the structures have low barriers to interconversion, or the conformation is of no consequence on properties such as redox potentials or electronic spectra. Preliminary data[27] of the solution EPR spectra of two of the neutral d^1 niobium complexes are similar to the results of Dahl and co-workers in studies of $Cp_2V(SC_6H_5)_2$.[4] The toluene solution spectra of $Cp_2Nb(S\text{-}p\text{-}C_6H_4Cl)_2$ and $Cp_2Nb(S\text{-}p\text{-}C_6H_4Me)_2$ show a 10-line hyperfine pattern due to the interaction of the unpaired electron with the ^{93}Nb nucleus ($I = {}^9/_2$, 100%) at g = 1.988548 (A = 97.159 Gaus) and g = 1.988944 (A = 97.0116 gaus), respectively. Since an unpaired electron in the SOMO of an endo vs exo configuration is expected to show a substantial difference in EPR parameters, the similarity of these values suggests the structures are the same in solution. Further studies are underway to contrast these data with magnetically dilute crystal data.[27]

Table IV. Structures of $Cp_2M(SR)_2$ Complexes where R = Alkyl or Aryl and M = Ti, V, Nb, or Mo

compd	d electrons	S–M–S, deg	ref
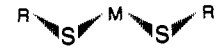			
exo conformation			
$Cp_2Nb(S\text{-}p\text{-}C_6H_4OMe)_2$	d^1	79.1	*a*
$Cp_2Nb(S\text{-}p\text{-}C_6H_4Me)_2$	d^1	77.1	*a*
$Cp_2Nb(SPh)_2$	d^1	75.4	1
$Cp_2Mo(S\text{-}t\text{-}Bu)_2$	d^2	71.1	8
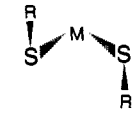			
endo conformation			
$Cp_2Nb(S\text{-}p\text{-}C_6H_4Cl)_2$	d^1	98.7	*a*
$Cp_2Nb(SPh)_2^+$	d^0	101.4	1
$Cp_2Nb(S\text{-}p\text{-}C_6H_4Cl)_2^+$	d^0	102.3	a
$Cp_2Ti(SMe)_2$	d^0	93.7	5
$Cp_2Ti(SEt)_2$	d^0	93.8	9
$Cp_2Ti(SPh)_2$	d^0	99.4	4
$Cp_2V(SPh)_2$	d^1	94.1	4
$Cp_2V(SMe)_2$	d^1	88.7	5a

[a] This work.

Barriers to inversion at S have been determined by dynamic NMR studies for S–aryls of some heterobimetallic complexes and for sulfur ring ligands of metallocenes. The $\Delta G^\ddagger$ for syn-anti conformational change in $syn\text{-}Cp_2Ti(\mu\text{-}SEt)_2CuPR_3$ is ~72 kJ/mol,[28] and such interconversion in $Cp_2Ti(\mu\text{-}SH)_2W(CO)_4$ was measured at 76 kJ/mol.[29] An estimate for the analogous process in $Cp_2Nb(\mu\text{-}SC_6H_5)_2Mo(CO)_4^+$ is on the order of 50 kJ/mol.[30] Free energies of activation have also been measured for MS_5 and MS_3 ring inversions in Cp_2MS_5 (M = Ti, Zr, Hf; $\Delta G^\ddagger$ = 76.3, 48.6, and 58.0 kJ/mol, respectively) and $(\eta^5\text{-}C_5(CH_3)_5)_2MS_3$ complexes (M = Ti and Zr; $\Delta G^\ddagger$ = 40.6 and 39.3 kJ/mol, respectively.)[31] Since it is reasonable that the barrier should be greater in these "tied-down" cases as opposed to the "free" S–R substituent, rapid interconversion of configurations in solution and a small difference, within the realm of crystal packing forces, between exo/endo configuration energies in the solid state is expected.

A reasonable test of the possibility that the observation of the endo conformation in the case of the *p*-chloro derivative is governed by crystal packing forces rather than a preference based on the electronic effects appeared to be the synthesis and structure of a complex containing a substituent more electron withdrawing than Cl, i.e., the $Cp_2Nb(S\text{-}p\text{-}C_6H_4CF_3)_2$ derivative.[32] Although

(27) Springs, J. J.; Williams, A. J.; Preston, K. F. Details of these results are to be published separately.
(28) Wark, T. A.; Stephan, D. W. *Inorg. Chem.* **1987**, *26*, 363.
(29) Ruffing, C. J.; Rauchfuss, T. B. *Organometallics* **1985**, *4*, 524.
(30) Simulations of ^1H NMR spectra are currently being carried out by S. A. Houliston in our labs.
(31) (a) Shaver, A.; McCall, J. M. *Organometallics* **1984**, *3*, 1823. (b) Shaver, A.; McCall, J. M.; Day, V. W.; Vollmer, S. *Can. J. Chem.* **1987**, *65*, 1676. (c) Shaver, A.; McCall, J. M. *J. Organomet. Chem.* **1980**, *193*, C37. (d) Shaver, A.; McCall, J. M. *Angew. Chem., Int. Ed. Engl.* **1982**, *21*, 384.

the quality of the crystal structure obtained for this complex is insufficient for publication due to twinning of crystals and possibly severe disorder in the CF_3 units, all indications are that the exo conformation prevails.[33] We conclude that apparently major changes in molecular conformation of these complexes arise from very minor differences in electronic distributions or overall energies. Detailed calculations with molecular orbital descriptions of the electronic distribution and conformer preferences are presented in a subsequent paper.[10]

Acknowledgment. The authors gratefully acknowledge the National Science Foundation (CHE86-03664) for financial support of this work. We are especially indebted to Prof. M. B. Hall for much helpful discussion and to Drs. J. J. Springs, A. J. Williams, and K. F. Preston for providing us with data prior to publication. The R3m/V single-crystal X-ray diffractometer and crystallographic computing system in the Crystal and Molecular Structures Laboratory at the Department of Chemistry, Texas A&M University was purchased from funds provided by the National Science Foundation (CHE-8513273). The VG analytical 70-s mass spectrometer was also purchased from funds provided by the NSF (CHE-870567). The scientific assistance of Dr. Thomas Sharp and Viji Dandapani are greatly appreciated.

Supplementary Material Available: Tables of atomic coordinates, bond lengths and angles, anisotropic displacement coefficients, and hydrogen atom coordinates, thermal ellipsoid plots, and packing diagrams for **2**, **3**, **4** and $\mathbf{4}^+$ (42 pages); listing of structure factor amplitudes (33 pages). Ordering information is given on any current masthead page.

(32) The $HSC_6H_4CF_3$ was prepared by the method given in the following: Wong, G. B.; Kurtz, D. M.; Holm, R. H.; Mortenson, L. E.; Upchurch, R. G. *J. Am. Chem. Soc.* **1979**, *101*, 3078. The $Cp_2Nb(S\text{-}p\text{-}C_6H_4CF_3)_2$ complex was synthesized by the same method as the other complexes. Elemental analysis: calcd C (49.92), H (3.14); found C (49.60), H (3.10).

(33) The molecular structure of $Cp_2Nb(S\text{-}p\text{-}C_6H_4CF_3)_2$ ($C_{24}H_{18}F_6S_2Nb$), M_r = 577.4, monoclinic, $P2_1/a$, a = 26.001 (11) Å, b = 13.805 (7) Å, c = 13.715 (6) Å, β = 112.53 (3)°, V = 4547 (4) Å^3, D_x = 1.687 g cm^{-3}, μ = 0.741 mm^{-1}, Z = 8, $F(000)$ = 2312 e$^-$, T = 193 K. Two unique molecules were present in the unit cell. 6475 reflections were collected on a Nicolet R3m diffractometer employing the θ–2θ scanning technique. A semiempirical absorption correction was applied (ellipsoid approximation; μ_{xr} = 0.15, T_{max} = 0.9855, T_{min} = 0.6477). A total of 2349 unique reflections ($I \geq 4.0\sigma I$) were employed by full-matrix least-squares refinement on F^2 to refine 262 parameters to convergence. Final R = 0.132, wR = 0.126, s = 3.55. Poor crystal quality and disorder in the CF_3 groups prevented publication quality results. The conformation of the $S\text{-}p\text{-}C_6H_4CF_3$ groups was exo [$(Nb\text{–}S)_{av}$ = 2.52 (1) Å, $(S\text{–}Nb\text{–}S)_{av}$ = 75.4 (2)°].

Solution Equilibrium between Classical and Nonclassical Polyhydride Tautomers $[ReH_4(CO)L_3]^+$ and $[ReH_2(\eta^2\text{-}H_2)(CO)L_3]^+$ (L = PMe_2Ph). Equilibrium Isotope Effects and an Intermediate Trihydrogen Complex in Intramolecular Site Exchange of Dihydrogen and Hydride Ligands

Xiao-Liang Luo* and Robert H. Crabtree

Contribution from the Department of Chemistry, Yale University, New Haven, Connecticut 06511. *Received March 14, 1990*

Abstract: Treatment of $ReCl_3(CO)(PMe_2Ph)_3$ with $LiAlH_4$ in refluxing Et_2O gives $ReH_3(CO)(PMe_2Ph)_3$ (**1**). Protonation of **1** with $HBF_4{\cdot}OEt_2$ in CD_2Cl_2 at −78 °C results in an equilibrium mixture of $[ReH_4(CO)(PMe_2Ph)_3]^+$ (**2a**) and its nonclassical tautomer $[ReH_2(\eta^2\text{-}H_2)(CO)(PMe_2Ph)_3]^+$ (**2b**). The site exchange of dihydrogen and hydride ligands in **2b** and the interconversion of **2a** and **2b** lead to an unusual temperature dependence of the T_1 values. **2b**-d_3 shows a $^1J_{HD}$ value of 34 Hz. An isotope effect is observed for the equilibrium between **2a** and **2b**; deuteration shifts the equilibrium toward the nonclassical form. In addition, an isotope fractionation is found in partially deuterated **2b**, with a substantial preference for deuterium to occupy the nonclassical site. These two processes can lead to isotopic perturbation of resonance (IPR) effects of opposite sign and constitute a new case in which expected IPR shifts are not observed. The hydride site exchange in **2b** is much faster than the interconversion of **2b** and **2a**, indicating that **2a** is *not* an intermediate in the former process. The intermediacy of a trihydrogen complex is therefore proposed for the site exchange in **2b**.

Introduction

Transition-metal polyhydride complexes L_yMH_x ($x \geq 4$)[1] have attracted much interest, not only because they represent examples of the stabilization of high formal oxidation states and high coordination numbers by the uniquely small hydride ligand, but also because they offer a rich and fascinating chemistry including C–H activation.[2] Following the discovery of η^2-H_2 coordination,[3] it is now well established[4-7] that polyhydrides may adopt classical structures having only terminal hydride ligands (e.g., WH_6L_3) or nonclassical structures with one or more η^2-H_2 ligands (e.g.,

(1) (a) Hlatky, G.; Crabtree, R. H. *Coord. Chem. Rev.* **1985**, *65*, 1. (b) Moore, D.; Robinson, S. D. *Chem. Soc. Rev.* **1983**, *12*, 415.

(2) (a) Crabtree, R. H. *Chem. Rev.* **1985**, *85*, 245. (b) Kelle Zeiher, E. H.; DeWit, D. G.; Caulton, K. G. *J. Am. Chem. Soc.* **1984**, *106*, 7006. (c) Aktogu, N.; Baudry, D.; Cox, D.; Ephritikhine, M.; Felkin, H.; Holmes-Smith, R.; Zakrzewski, J. *Bull. Soc. Chim. Fr.* **1985**, 381.

(3) (a) Kubas, G. J. *Acc. Chem. Res.* **1988**, *21*, 120. (b) Crabtree, R. H.; Hamilton, D. G. *Adv. Organomet. Chem.* **1988**, *28*, 299. (c) Crabtree, R. H. *Acc. Chem. Res.* **1990**, *23*, 95.

(4) (a) Crabtree, R. H.; Lavin, M. *J. Chem. Soc., Chem. Commun.* **1985**, 1661. (b) Crabtree, R. H.; Lavin, M.; Bonneviot, L. *J. Am. Chem. Soc.* **1986**, *108*, 4032.

(5) (a) Crabtree, R. H.; Hamilton, D. G. *J. Am. Chem. Soc.* **1986**, *108*, 3124. (b) Hamilton, D. G.; Crabtree, R. H. *J. Am. Chem. Soc.* **1988**, *110*, 4126. (c) Luo, X.-L.; Crabtree, R. H. *Inorg. Chem.* **1990**, *29*, 2788.

(6) Arliguie, T. A.; Chaudret, B.; Morris, R. H.; Sella, A. *Inorg. Chem.* **1988**, *27*, 599.

(7) (a) Lundquist, E. G.; Huffman, J. C.; Folting, K.; Caulton, K. G. *Angew. Chem., Int. Ed. Engl.* **1987**, *27*, 1165. (b) Lundquist, E. G.; Folting, K.; Streib, W. E.; Huffman, J. C.; Eisenstein, O.; Caulton, K. G. *J. Am. Chem. Soc.* **1990**, *112*, 855. (c) Johnson, T. J.; Huffman, J. C.; Caulton, K. G.; Jackson, S. A.; Eisenstein, O. *Organometallics* **1989**, *8*, 2073. (d) Van Der Sluys, L. S.; Eckert, J.; Eisenstein, O.; Hall, J. H.; Huffman, J. C.; Jackson, S. A.; Koetzle, T. F.; Kubas, G. J.; Vergamini, P. J.; Caulton, K. G. *J. Am. Chem. Soc.* **1990**, *112*, 4831.

0002-7863/90/1512-6912$02.50/0